Dipolar interactions in F=1 ferromagnetic spinor condensates. Roton instabilities and possible supersolid phase

Eugene Demler Harvard University

Collaboration with Robert Cherng
Thanks to Vladimir Gritsev, Dan Stamper-Kurn

Funded by NSF, DARPA, MURI, AFOSR, Harvard-MIT CUA

Outline

Introduction

Dipolar interactions averaged over
fast Larmor precession

Instabilities: qualitative picture

Instabilities: roton softening and phase diagram

Instabilities of the spiral state

Introduction:
Roton excitations and supersolid phase

Theory of the Superfluidity of Helium II

L. Landau

From these properties of the energy spectrum the heat capacity of helium II must consist of two parts: the "phonon part," i.e., the normal Debye heat capacity proportional to T^4, and the "roton part," depending on the temperature exponentially $(\sim e^{-\Delta/kT})$.

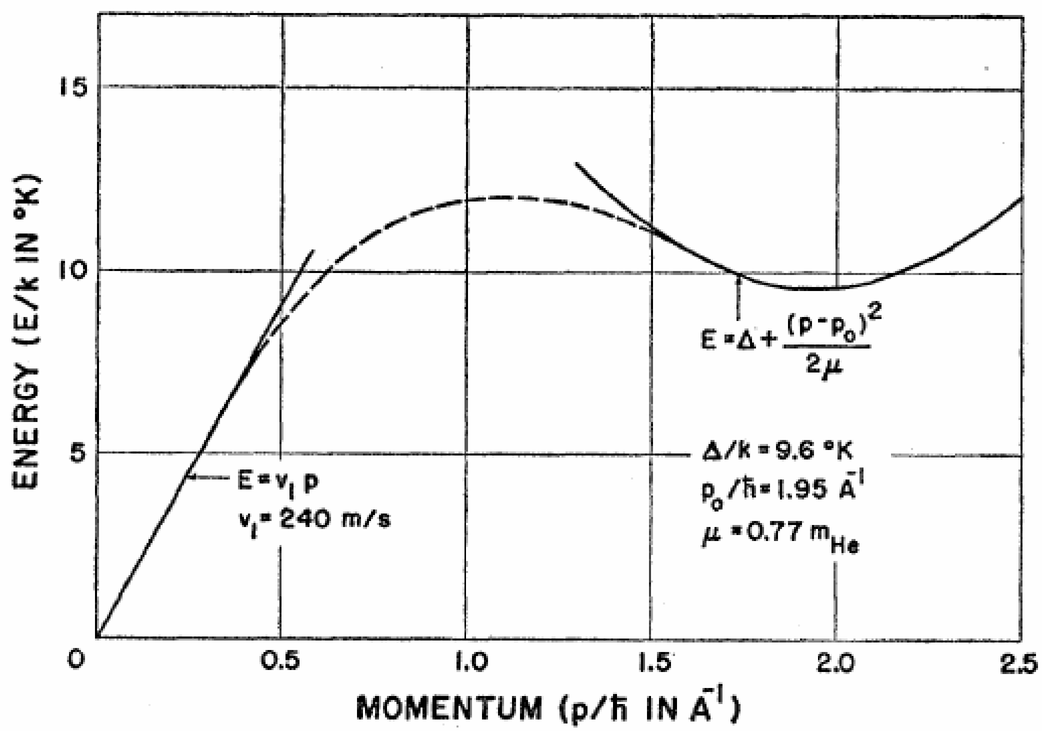

Energy Spectrum of the Excitations in Liquid Helium*

R. P. FEYNMAN AND MICHAEL COHEN

A wave function previously used to represent an excitation (phonon or roton) in liquid helium, inserted into a variational principle for the energy, gave an energy-momentum curve having the qualitative shape suggested by Landau; but the value computed for the minimum energy Δ of a roton was 19.1°K, while thermodynamic data require $\Delta=9.6$°K. A new wave function is proposed here. The new value computed for Δ is 11.5°K. Qualitatively, the wave function suggests that the roton is a kind of quantum-mechanical analog of a microscopic vortex ring, of diameter about equal to the atomic spacing. A forward motion of single atoms through the center of the ring is accompanied by a dipole distribution of returning flow far from the ring.

FIG. 6. The energy spectrum of excitations. Curve A is the spectrum $E_2(k)$ computed from Eq. (61). Curve B is the spectrum $E_1(k)$ computed with the simpler wave function (5). Curve C is the Landau-type spectrum used by de-Klerk *et al.*[4] to fit the second sound and specific heat data. Curve D is a Landau-type spectrum with p_0 taken the same as in A, and μ and Δ chosen to fit the specific heat data. For small k, all curves are asymptotic to the line $E=\hbar ck$.

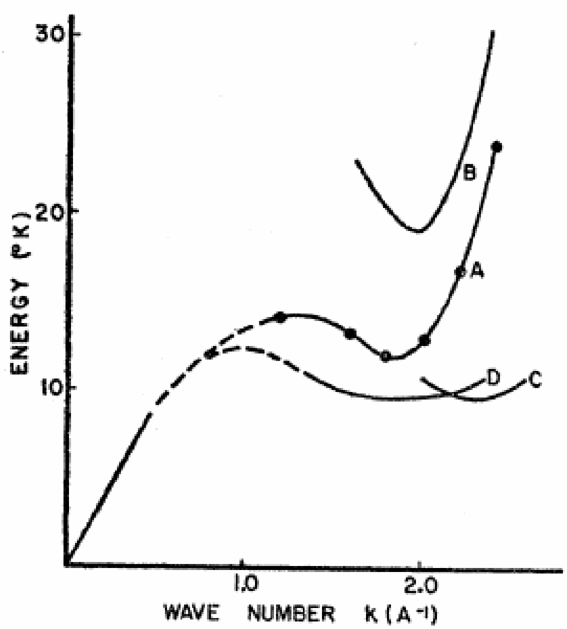

Excitations in Liquid Helium: Neutron Scattering Measurements*

J. L. Yarnell, G. P. Arnold, P. J. Bendt, and E. C. Kerr

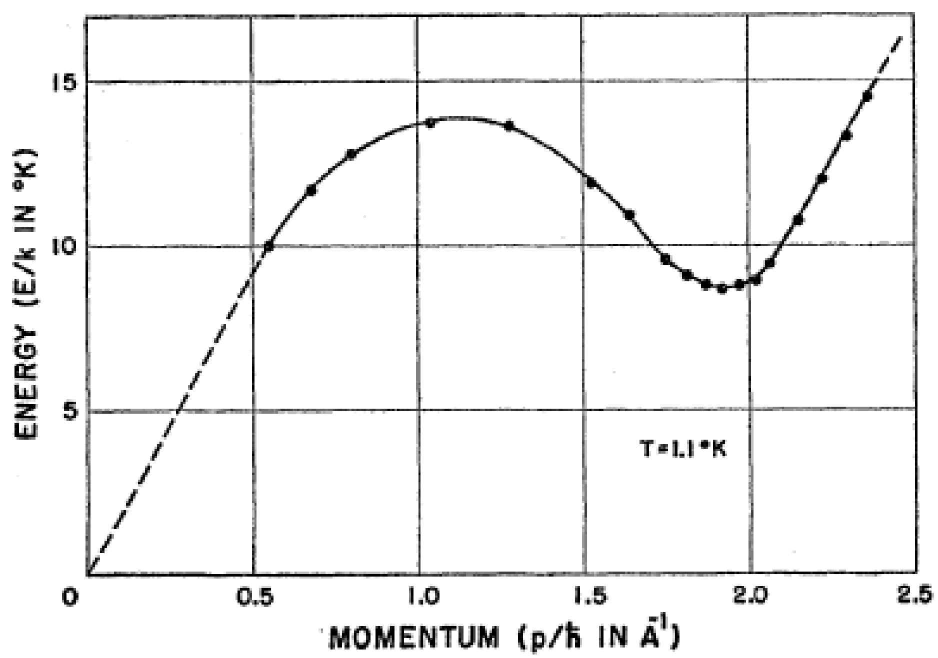

Fig. 8. The energy spectrum of the excitations in liquid helium at 1.1°K. The dashed line joining the origin and the first measured point has a slope corresponding to a first sound velocity of 239±5 meters/sec. The maximum occurs at $p/\hbar = 1.11 \pm 0.04$ A^{-1}, $E/k = 13.92 \pm 0.10$°K. The region of the minimum is shown in greater detail in Fig. 9.

Possible supersolid phase in ^{4}He

Phase diagram of 4He

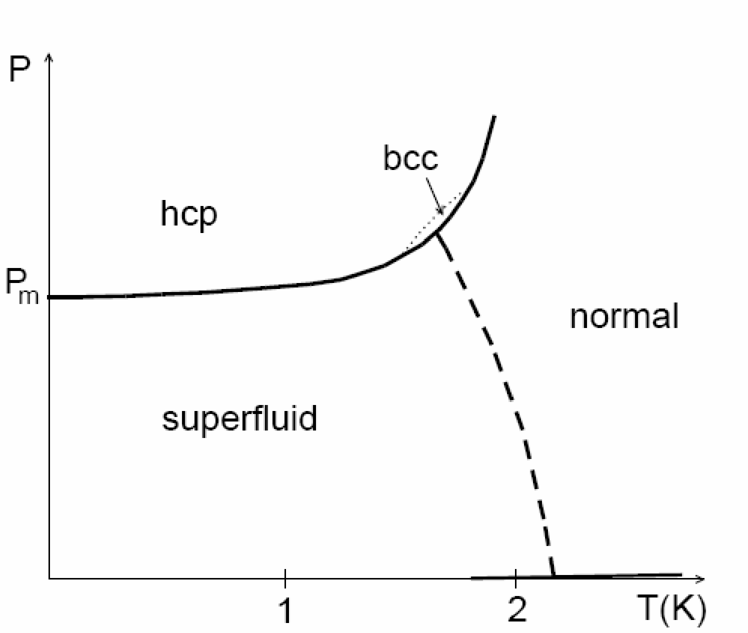

A.F. Andreev and I.M. Lifshits (1969):
Melting of vacancies in a crystal due to strong quantum fluctuations.

Also
G. Chester (1970); A.J. Leggett (1970)

T. Schneider and C.P. Enz (1971).
Formation of the supersolid phase due to softening of roton excitations

Probable observation of a supersolid helium phase

E. Kim & M. H. W. Chan

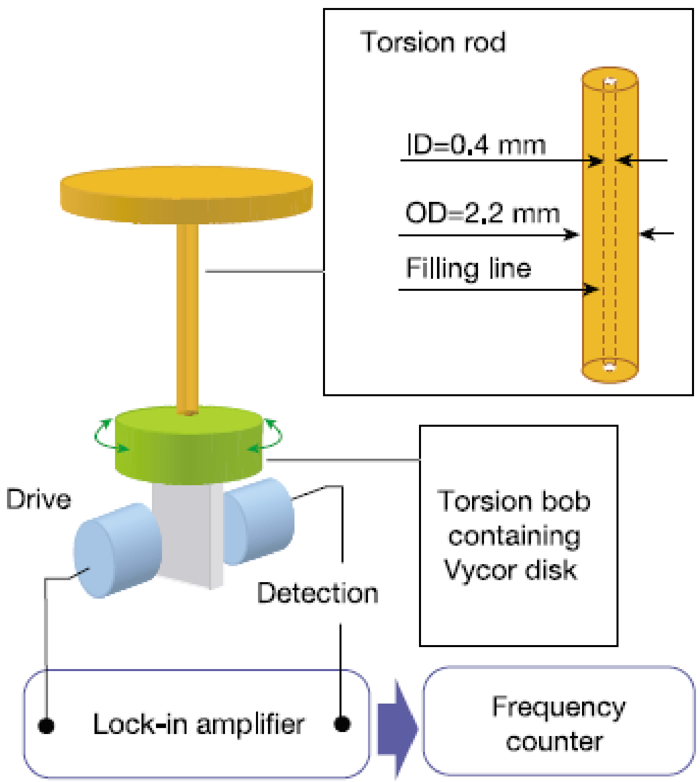

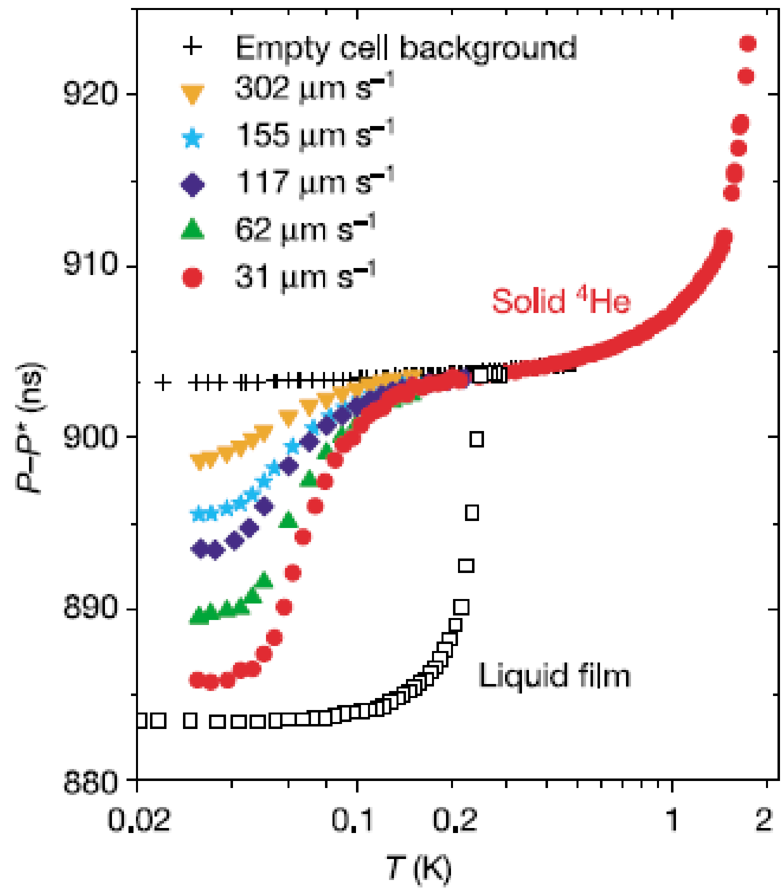

Resonant period as a function of T

Phases of bilayer quantum Hall systems at ν=1

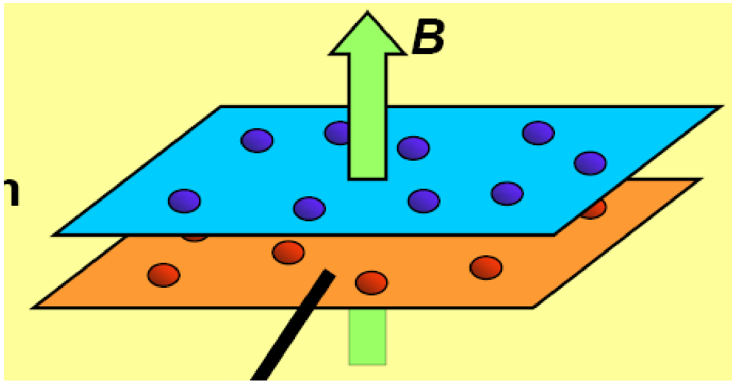

Hartree-Fock predicts roton softening and transition into the QH state with stripe order. Transport experiments suggest first order transition into a compressible state

Eisenstein, Boebinger et al. (1994)

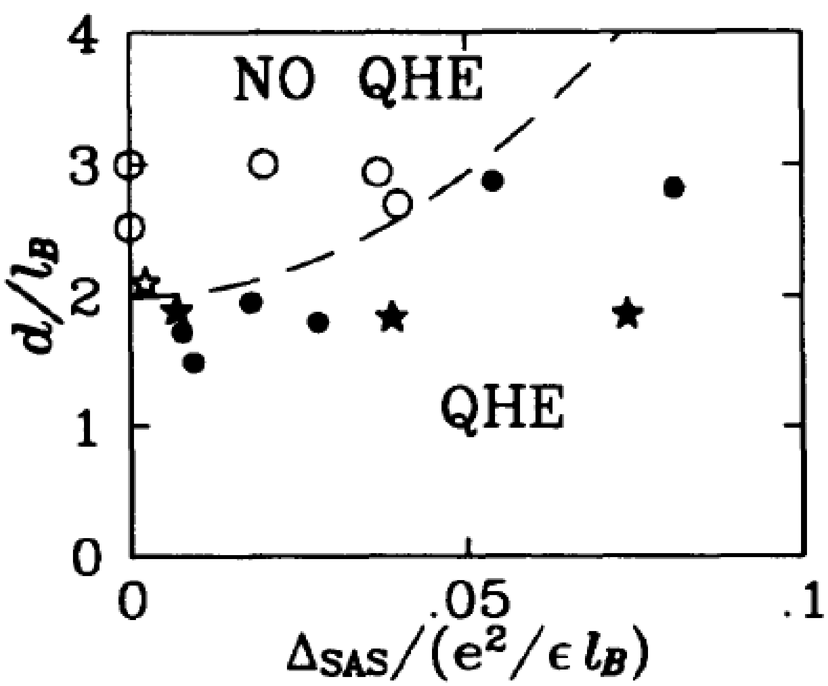

L. Brey and H. Fertig (2000)

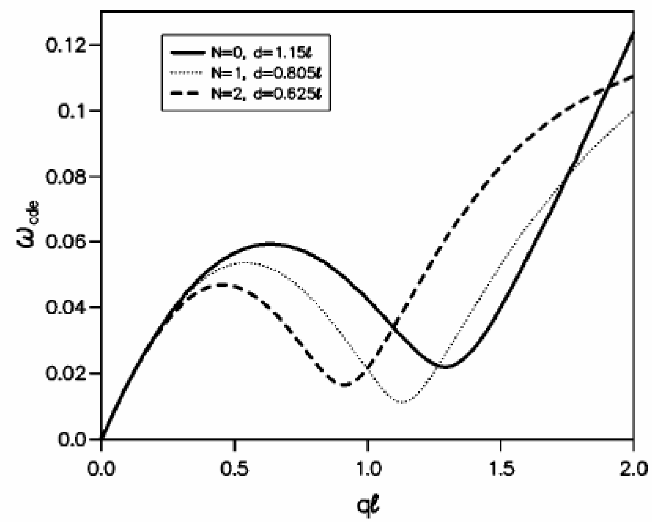

Phases of bilayer quantum Hall systems at ν=1 and roton softening

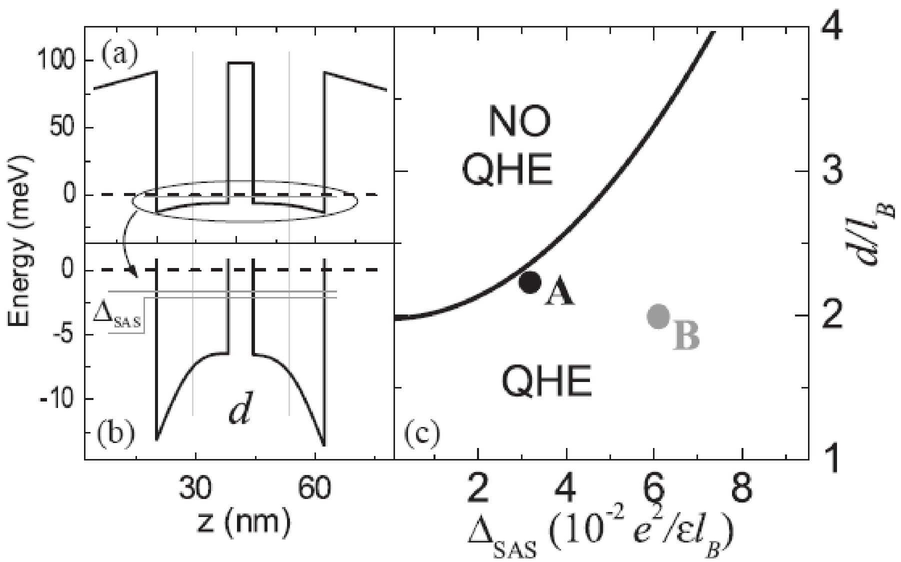

Raman scattering
Pellegrini, Pinczuk et al. (2004)

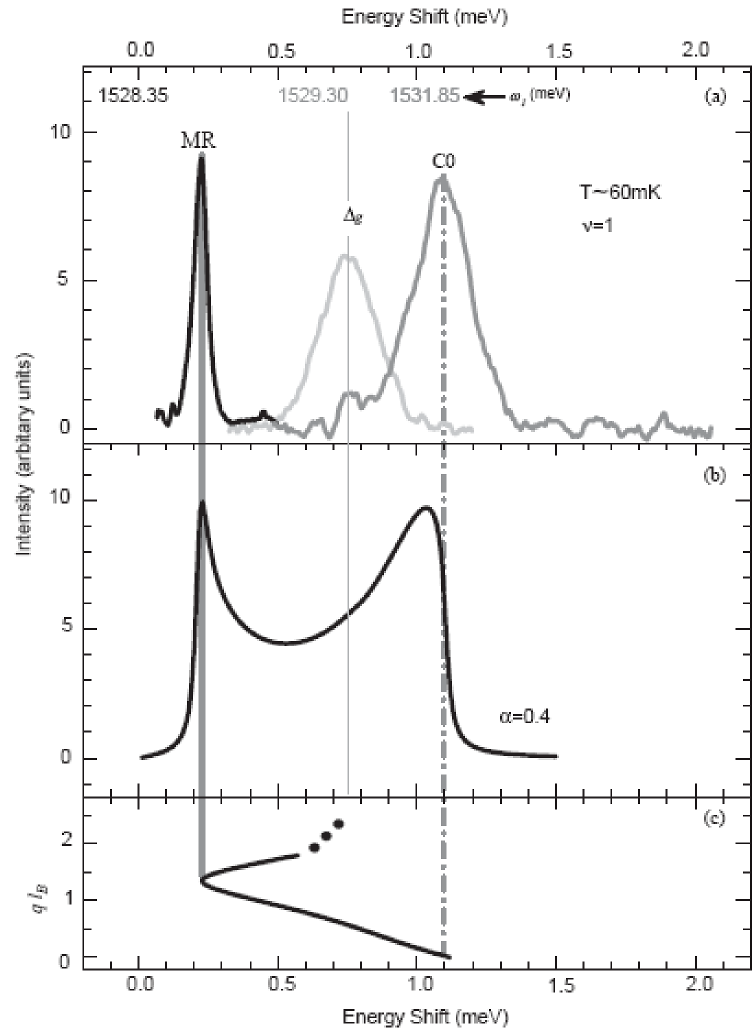

Roton softening and sharpening observed in Raman experiments. This is in conflict with transport measurements

Roton spectrum in pancake polar condensates

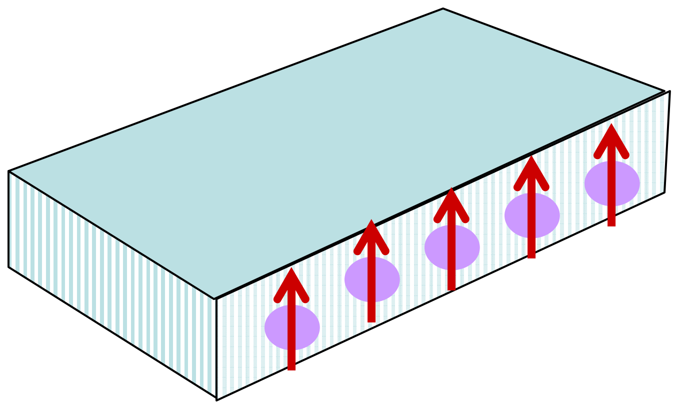

Santos, Shlyapnikov, Lewenstein (2000)
Fischer (2006)

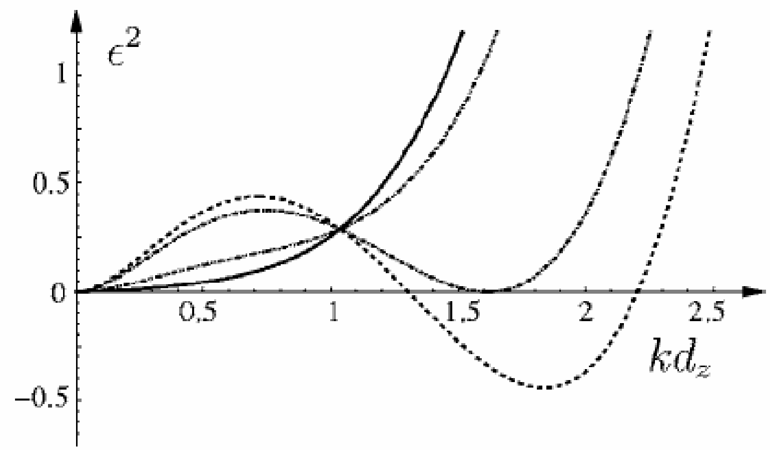

Origin of roton softening

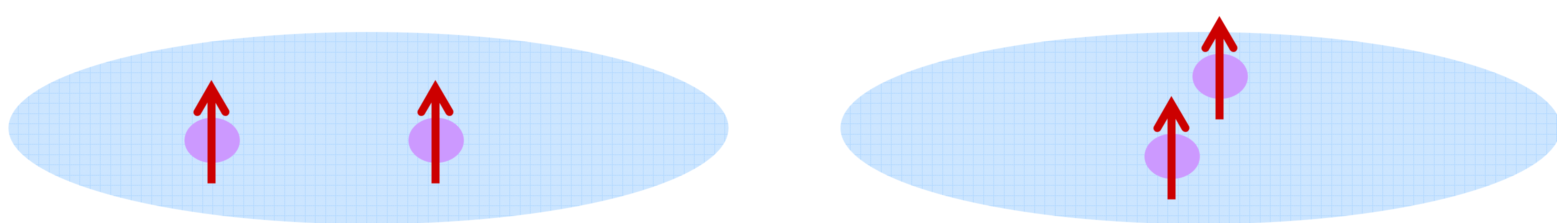

Repulsion at long distances

Attraction at short distances

Stability of the supersolid phase is a subject of debate

Magnetic dipolar interactions in spinor condensates

$$U_{\text{contact}}(\mathbf{r}) = \frac{4\pi\hbar^2 a}{m}\delta(\mathbf{r}) \quad V_{\text{dd}} = \frac{\mu_0\mu^2}{4\pi r^3}(1 - \cos\theta)$$

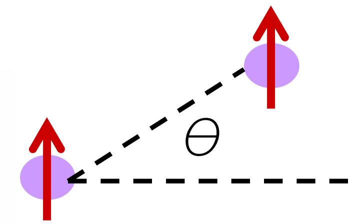

Comparison of contact and dipolar interactions.
Typical value a=100a_B

$$\epsilon = \frac{\mu_0\mu^2 m}{12\pi\hbar^2 a}$$

For ^{87}Rb μ=1/2μ_B and ϵ=0.007

For ^{52}Cr μ=6μ_B and ϵ=0.16

Bose condensation
of ^{52}Cr.
T. Pfau et al. (2005)

Review:
Menotti et al.,
arXiv 0711.3422

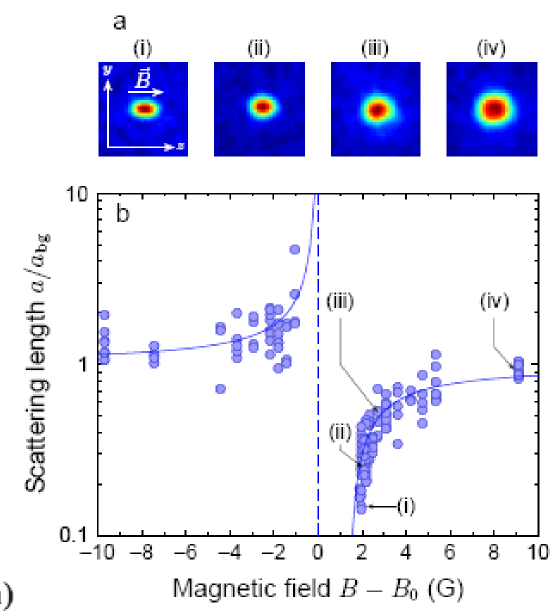

(a)

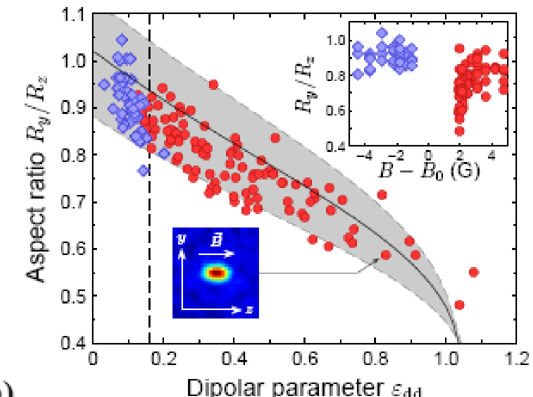

(b)

Magnetic dipolar interactions in spinor condensates

Interaction of F=1 atoms

$$V_S = c_0 + c_2 \vec{f}_1 \cdot \vec{f}_2$$

$$c_2 \equiv (4\pi\hbar^2/M) \times (a_2 - a_0)/3$$

Ferromagnetic Interactions for ^{87}Rb

a_2-a_0= -1.07 a_B

A. Widera, I. Bloch et al.,
New J. Phys. 8:152 (2006)

Spin-depenent part of the interaction is small.
Dipolar interaction may be important (D. Stamper-Kurn)

Spontaneously modulated textures in spinor condensates

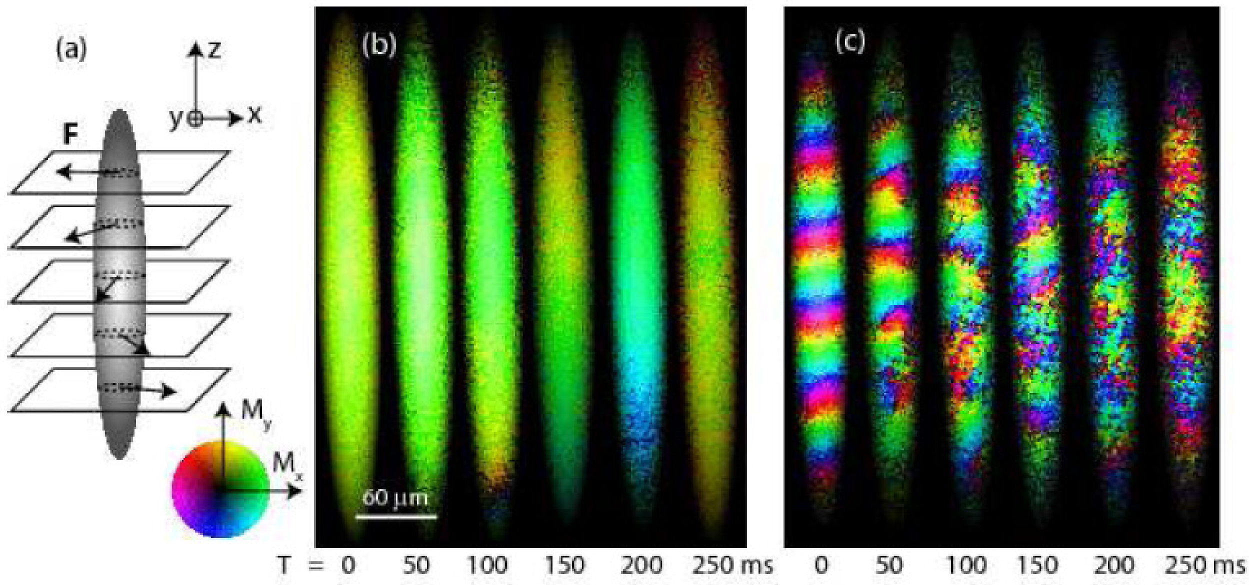

Vengalattore et al.
PRL (2008)

Fourier spectrum of the fragmented condensate

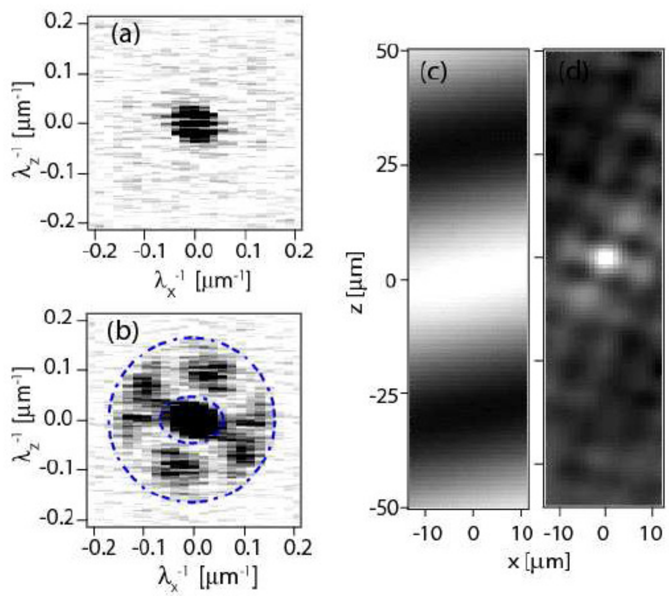

This talk: Instabilities of F=1 spinor condensates due to dipolar interactions. New phenomena due to averaging over Larmor precession

Theory: unstable modes in the regime corresponding to Berkeley experiments

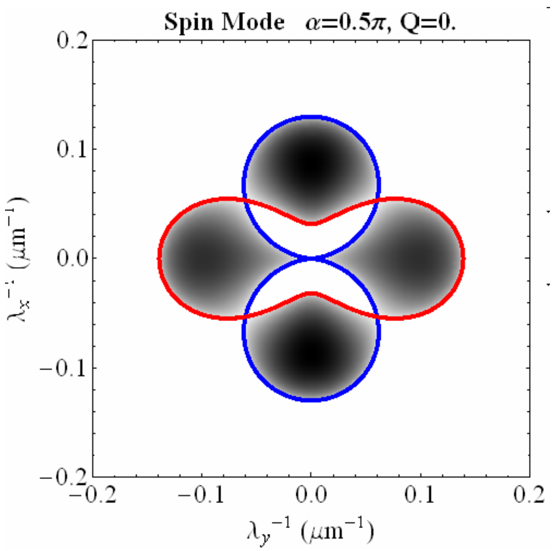

Results of Berkeley experiments

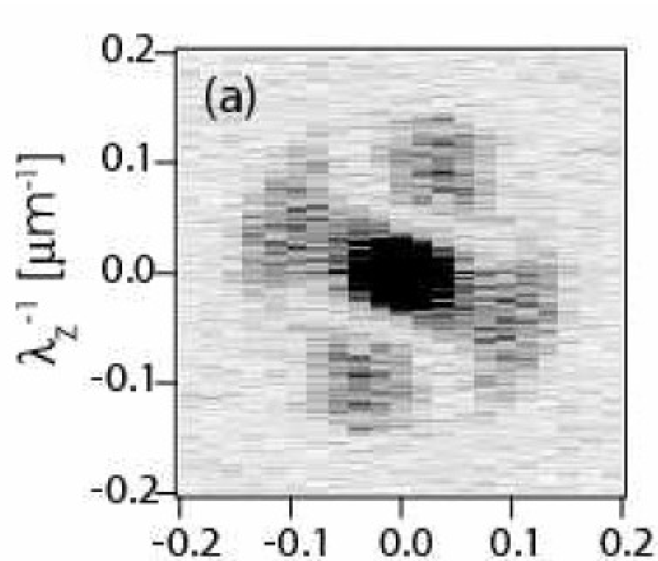

Wide range of instabilities tuned by quadratic Zeeman, AC Stark shift, initial spiral spin winding

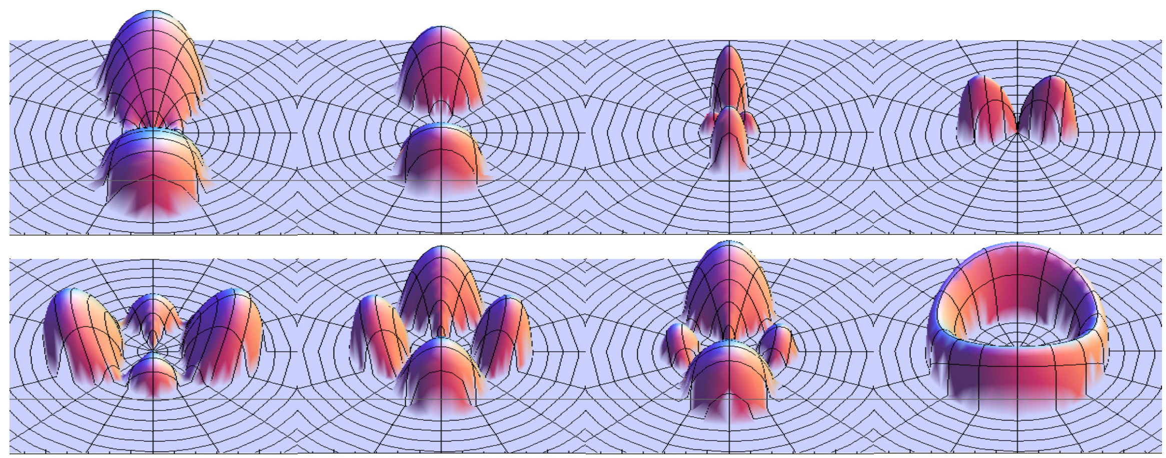

Instabilities of F=1 spinor condensates due to dipolar interactions and roton softening

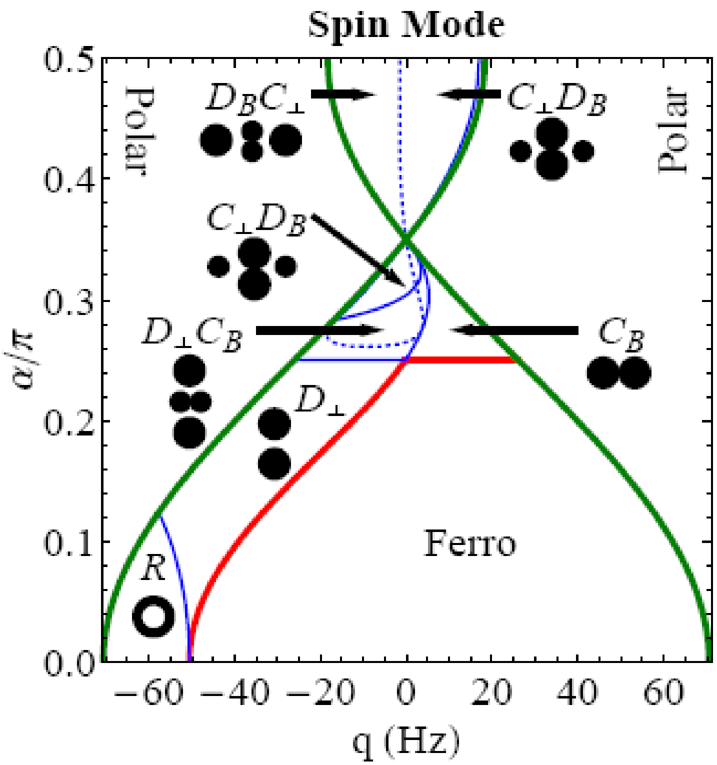

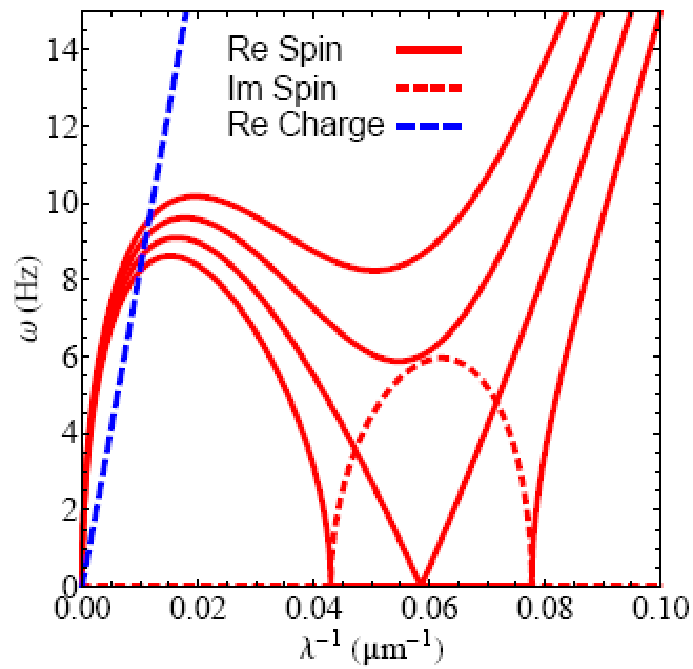

Earlier theoretical work on dipolar interactions in spinor condensates: Meystre et al. (2002), Ueda et. al. (2006), Lamacraft (2007).

New phenomena: interplay of finite transverse size and dipolar interaction in the presence of fast Larmor precession

Dipolar interactions after averaging over Larmor precession

Energy scales

Magnetic Field

- Larmor Precession (10 kHz)
- Quadratic Zeeman (0-20 Hz)

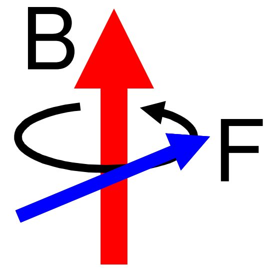

S-wave Scattering

- Spin independent ($g_0 n$ = kHz)
- Spin dependent ($g_s n$ = 10 Hz)

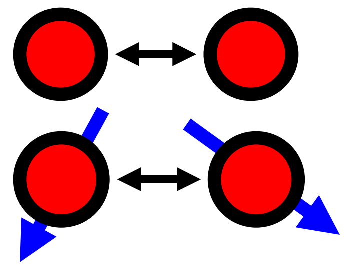

Dipolar Interaction

- Anisotropic ($g_d n$=10 Hz)
- Long-ranged

Reduced Dimensionality

- Quasi-2D geometry

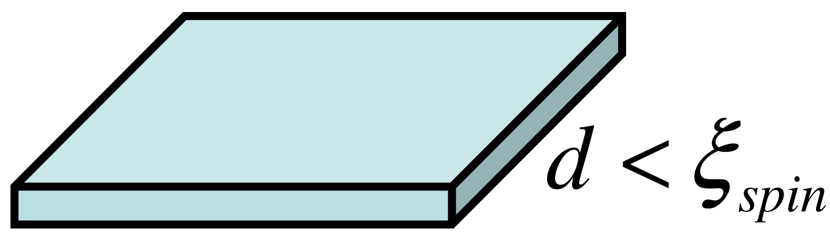

Dipolar interactions

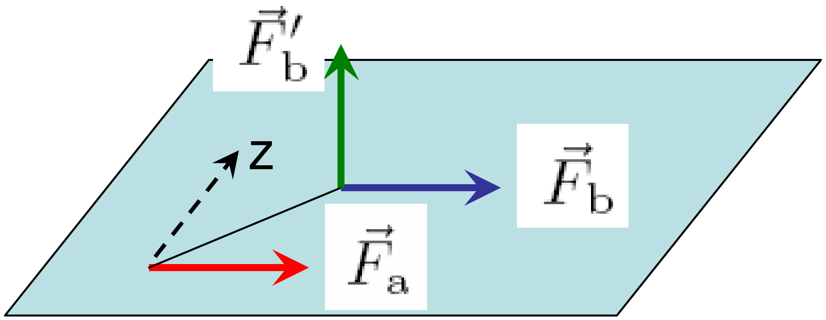

Static interaction

$\vec{F}_{\rm b}$ parallel to $\vec{F}_{\rm a}$ is preferred

"Head to tail" component dominates

Averaging over Larmor precession

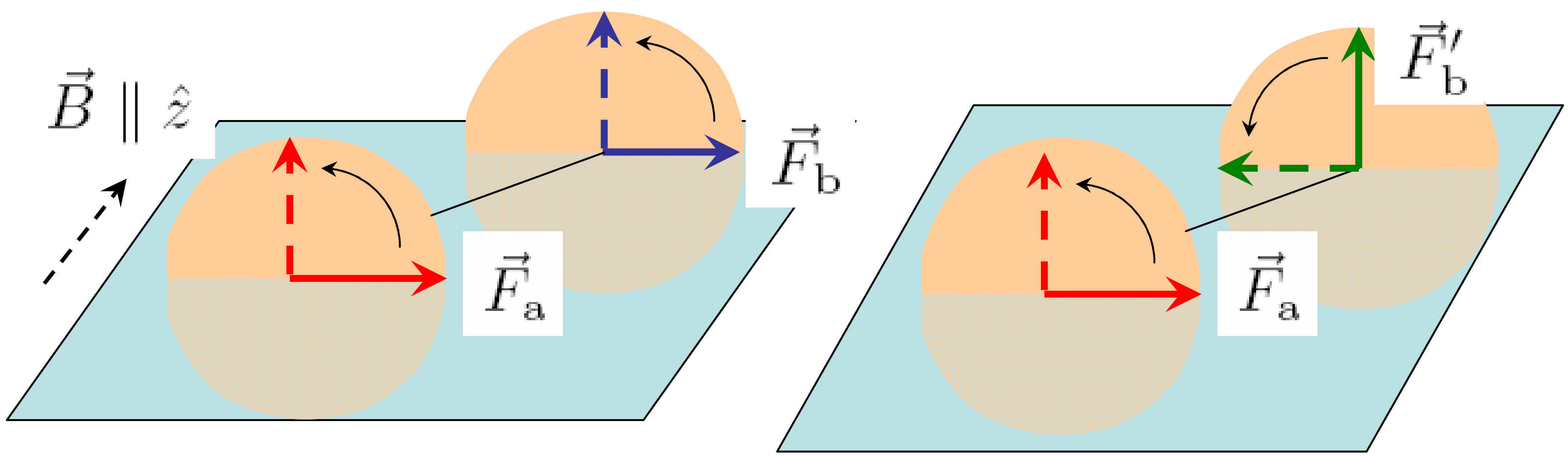

$\vec{F}'_{\rm b}$ perpendicular to $\vec{F}_{\rm a}$ is preferred. "Head to tail" component is averaged with the "side by side"

Instabilities: qualitative picture

Stability of systems with static dipolar interactions

Ferromagnetic configuration is robust against small perturbations. Any rotation of the spins conflicts with the “head to tail” arrangement

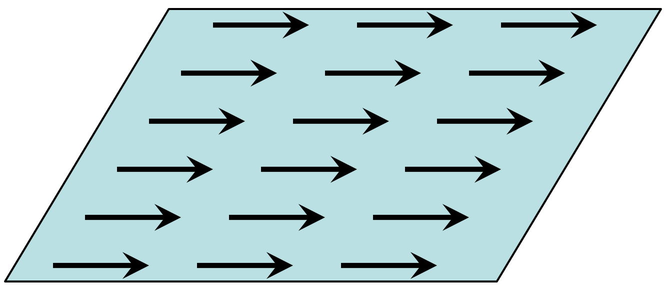

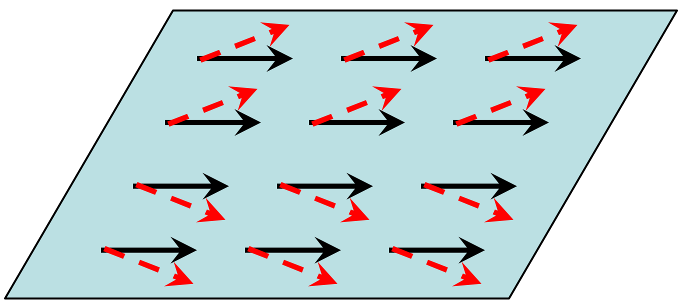

Large fluctuation required to reach a lower energy configuration

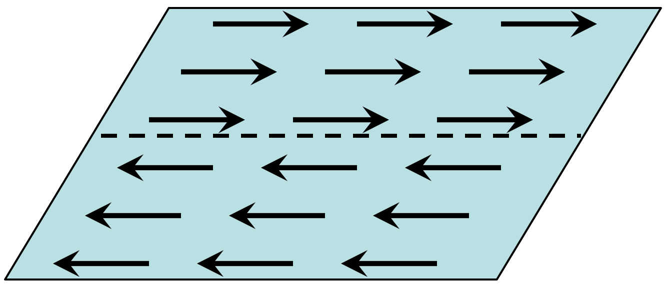

Dipolar interaction averaged after precession

“Head to tail” order of the transverse spin components is violated by precession. Only need to check whether spins are parallel

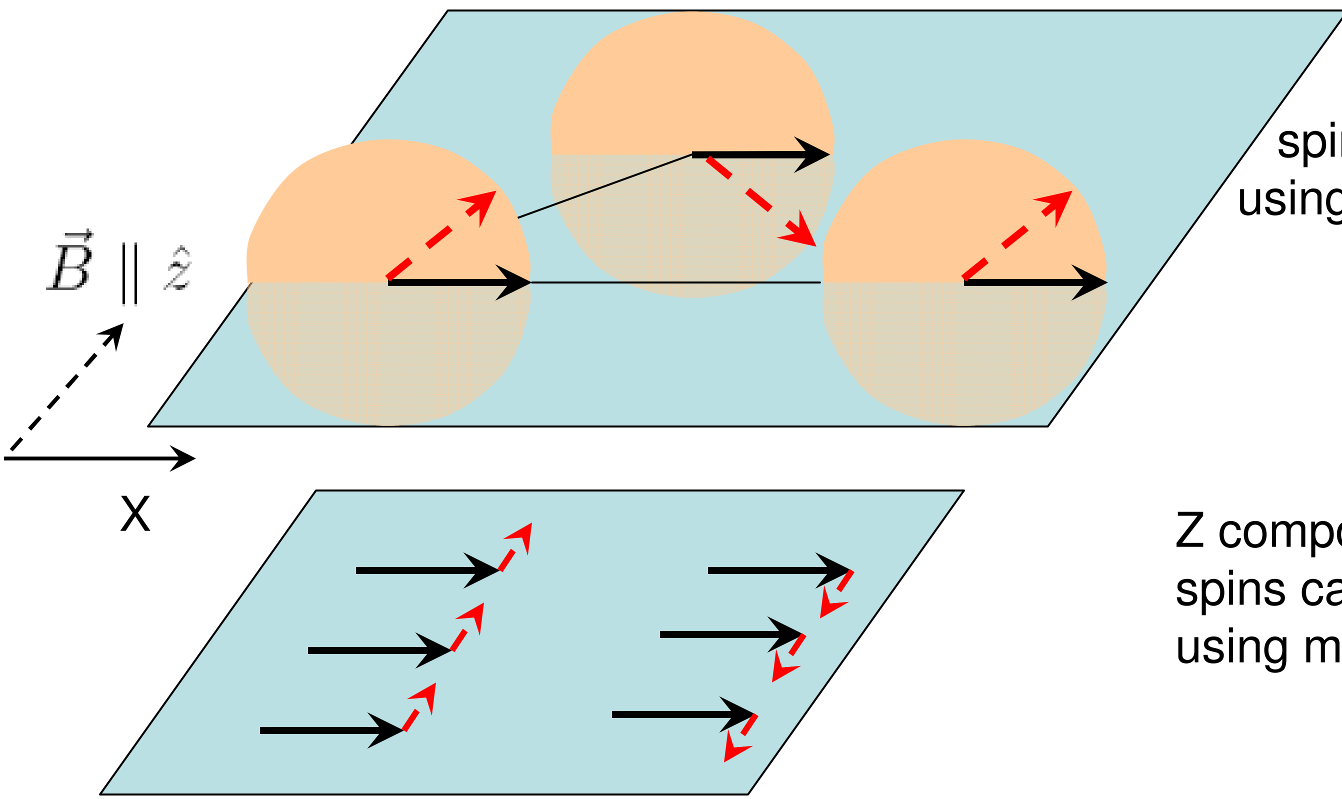

XY components of the spins can lower the energy using modulation along z.

Z components of the spins can lower the energy using modulation along x

Strong instabilities of systems with dipolar interactions after averaging over precession

Instabilities: technical details

From Spinless to Spinor Condensates

$$\langle \Psi \rangle = \sqrt{n} e^{i\phi} \qquad \langle \Psi \rangle = \sqrt{n} \left[\Phi_x, \Phi_y, \Phi_z \right]$$

$$\Psi = \sqrt{n} \begin{bmatrix} i e^{i\eta + i\eta_\perp} \cos(\phi + i\chi) \frac{\sin(\rho)}{\sqrt{\cosh(2\chi)}} \\ i e^{i\eta + i\eta_\perp} \sin(\phi + i\chi) \frac{\sin(\rho)}{\sqrt{\cosh(2\chi)}} \\ e^{i\eta} \cos(\rho) \end{bmatrix}$$

Charge mode:

n is density and η is the overall phase

Spin mode:

ϕ determines spin orientation in the XY plane

χ determines longitudinal magnetization (Z-component)

Hamiltonian

Quasi-2D

Magnetic Field

$$\mathcal{H} = \int d^3x \boldsymbol{\Psi}_x^\dagger \left[-\frac{\nabla^2}{2m} - \mu + \boxed{\frac{1}{2}\omega_n^2 \left(\hat{n}\cdot\vec{x}\right)^2} + \boxed{(-p + B_0)\left(\hat{B}\cdot\vec{F}\right) + q\left(\hat{B}\cdot\vec{F}\right)^2} \right] \boldsymbol{\Psi}_x$$

$$+ \int d^3x d^3x' \frac{1}{2} g_{3D}^{\mu\nu}(x - x') : (\boldsymbol{\Psi}_x^\dagger F^\mu \boldsymbol{\Psi}_x)(\boldsymbol{\Psi}_{x'}^\dagger F^\nu \boldsymbol{\Psi}_{x'}) :$$

Dipolar Interaction

$$g_{3D}^{ij}(\Delta x) = -g_s \delta^{ij} \delta(\Delta x) + \boxed{g_d \frac{1}{|\Delta x|^3} \left[\delta^{ij} - 3\Delta\hat{x}^i \Delta\hat{x}^j\right]}$$

S-wave Scattering

$$g_{3D}^{00}(\Delta x) = \boxed{(g_0 + g_s)\delta(\Delta x)}$$

$$(F^0)_{jk} = \delta_{jk}$$

$$(F^i)_{jk} = -i\epsilon_{ijk}$$

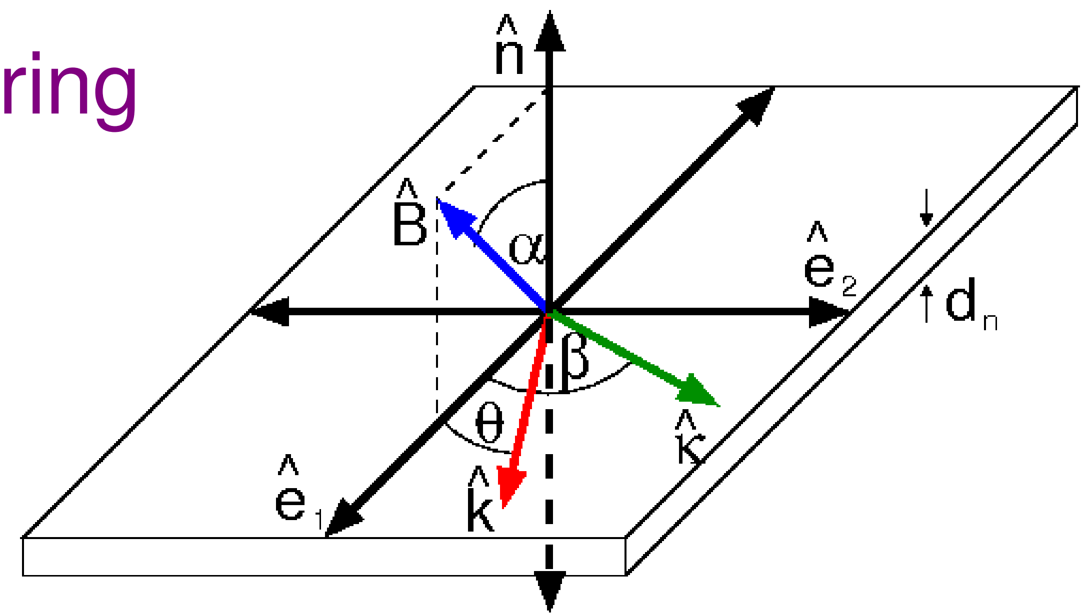

Precessional and Quasi-2D Averaging

Rotating Frame

$$\mathbf{\Psi} \rightarrow R(t,x)\mathbf{\Psi}$$

$$R(t,x) = \exp\left[i(B_0 t + \vec{\kappa}\cdot\vec{x})\hat{B}\cdot\vec{F}\right]$$

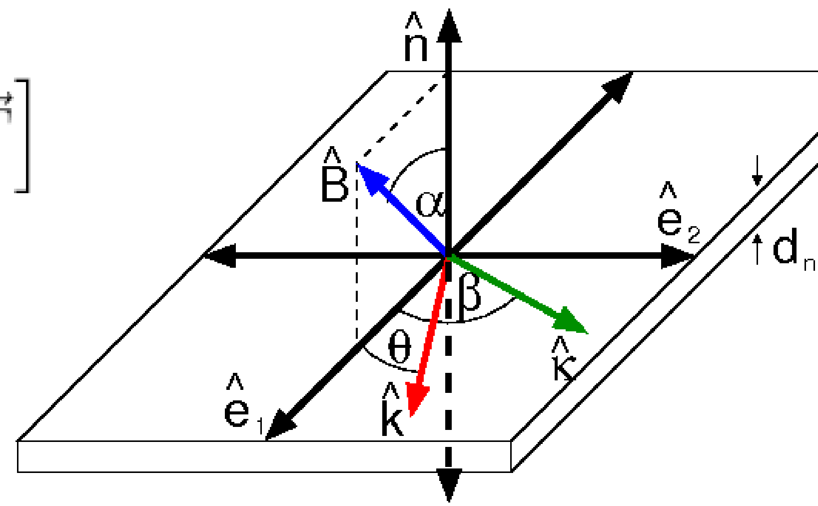

Gaussian Profile

$$\mathbf{\Psi}(x_1\hat{e}_1 + x_1\hat{e}_2 + x_n\hat{n}) =$$

$$\frac{e^{-x_n^2/4d_n^2}}{(2\pi d_n^2)^{1/4}}\mathbf{\Psi}(x_1\hat{e}_1 + x_2\hat{e}_2)$$

Quasi-2D Time Averaged Dipolar Interaction

$$(\delta^{ij} - 3\Delta\hat{x}^i\Delta\hat{x}^j) \rightarrow \int_{-\infty}^{\infty}\frac{d(\hat{n}\cdot\Delta\vec{x})}{2\sqrt{\pi}d_n}e^{-(\hat{n}\cdot\Delta\vec{x})^2/4d_n^2}\int_{-\pi/B_0}^{\pi/B_0}B_0 dt$$

$$\left[R(t,x)^T_{ii'}\left(\delta^{i'j'} - 3\Delta\hat{x}^{i'}\Delta\hat{x}^{j'}\right)R(t,x')_{j'j}\right]$$

Collective Modes

Mean Field

$$\Psi = \boxed{\Psi_0} + \boxed{\boxed{\delta\Psi}}$$

Collective Fluctuations
(Spin, Charge)

Equations of Motion

$$i\partial_t \begin{bmatrix} \delta\Psi_k \\ \delta\Psi^*_{-k} \end{bmatrix} = \begin{bmatrix} M_k & N_k \\ -N^*_{-k} & -M^*_{-k} \end{bmatrix} \begin{bmatrix} \delta\Psi_k \\ \delta\Psi^*_{-k} \end{bmatrix}$$

$$\delta\Psi(x,t) \sim \exp(i\omega_k - ikx)$$

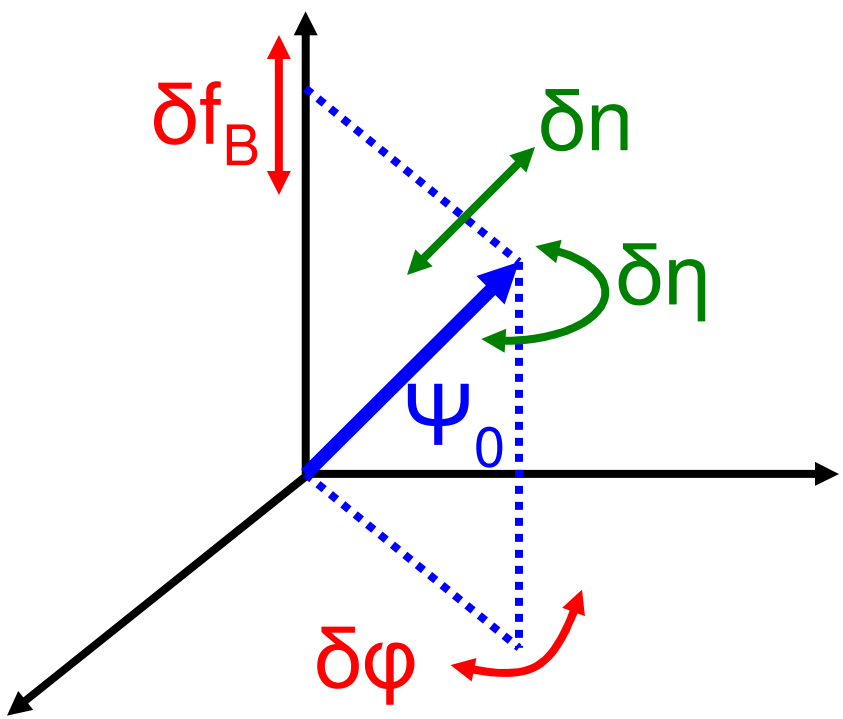

Spin Mode

δf_B – longitudinal magnetization
$\delta\varphi$ – transverse orientation

Charge Mode

δn – 2D density
$\delta\eta$ – global phase

Instabilities of collective modes

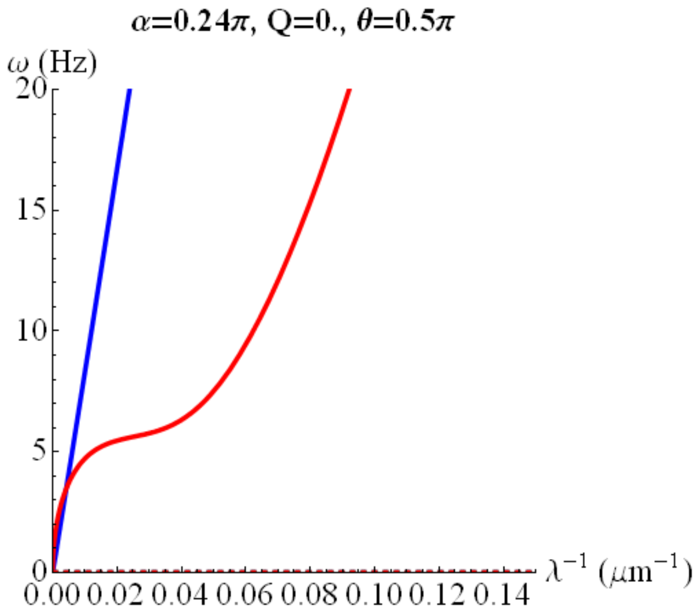

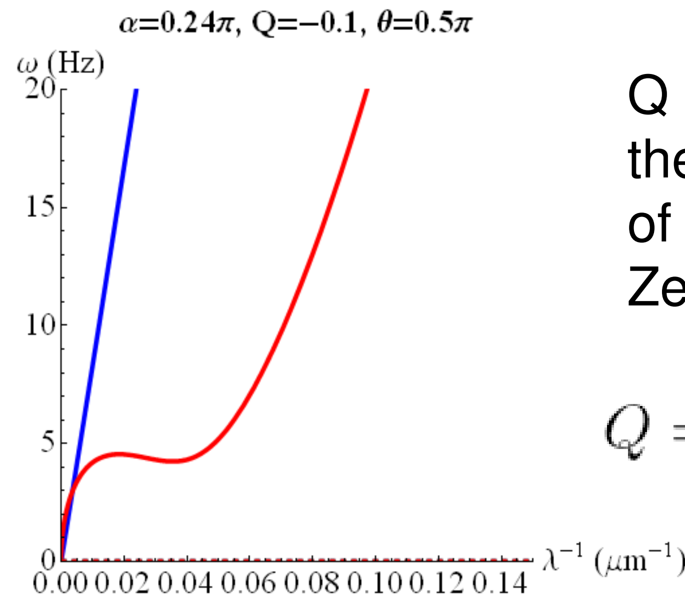

Q measures the strength of quadratic Zeeman effect

$$Q = -\frac{q}{2g^{\perp} n_{2D}}$$

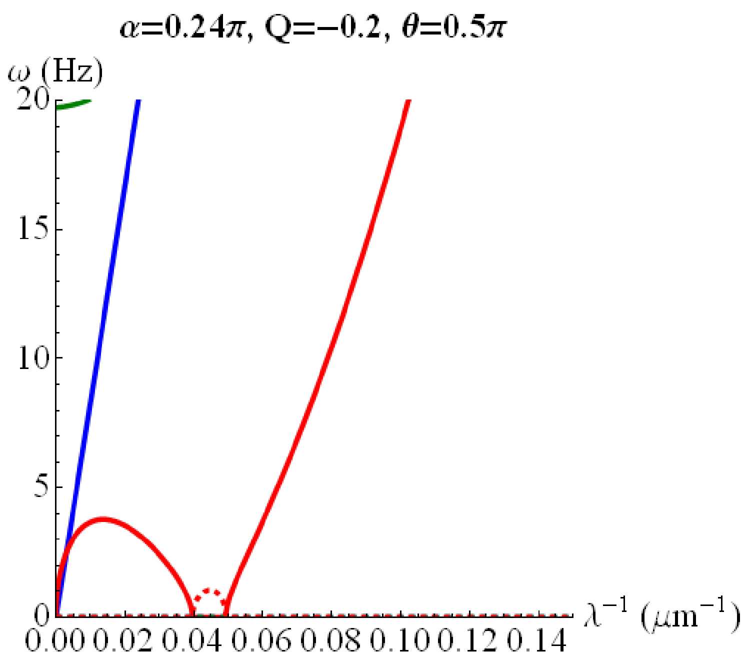

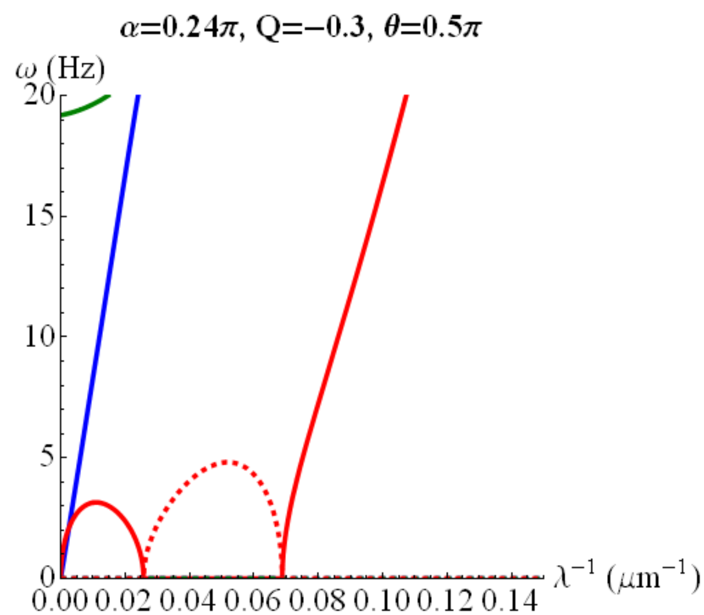

Instabilities of collective modes

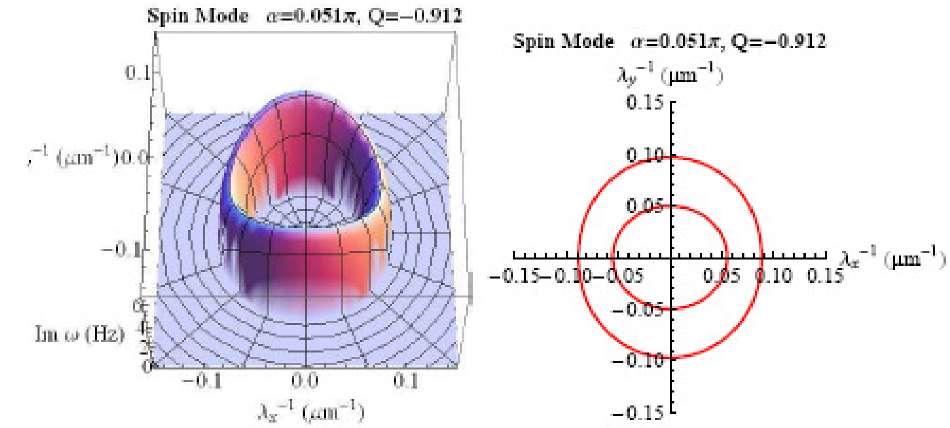

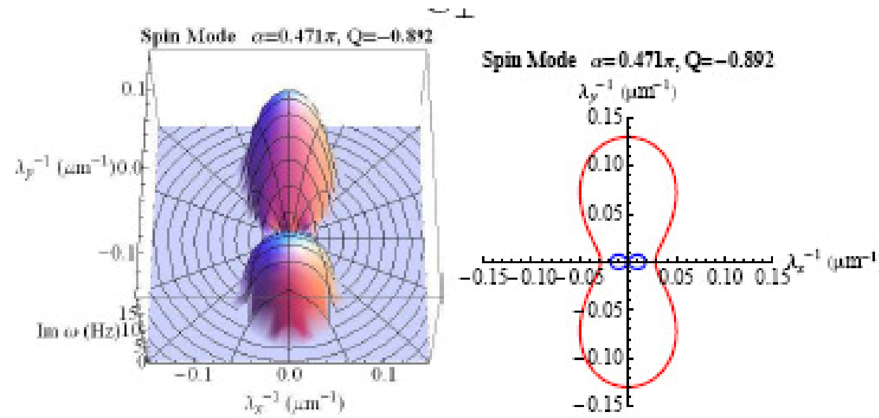

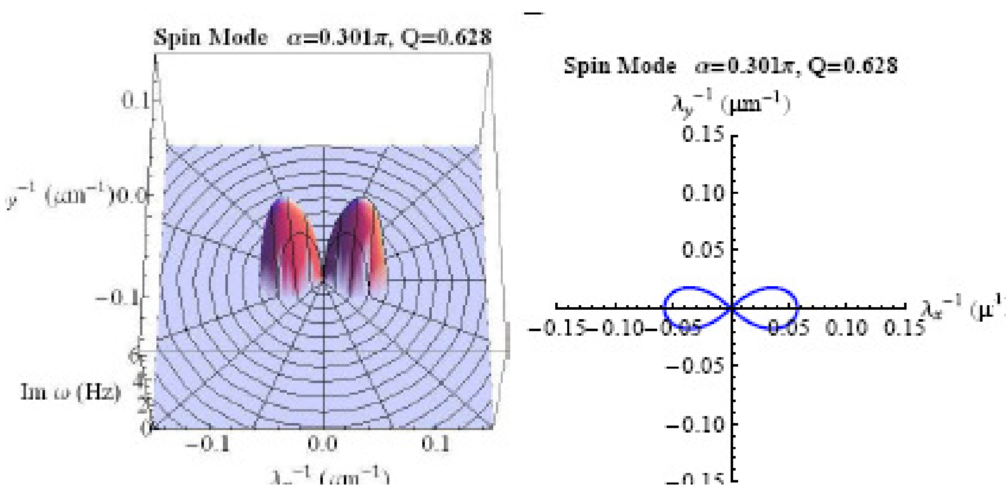

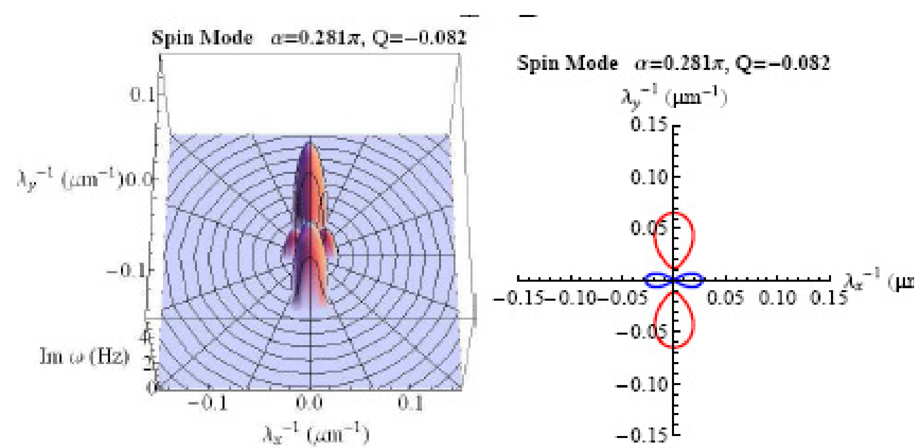

Berkeley Experiments: checkerboard phase

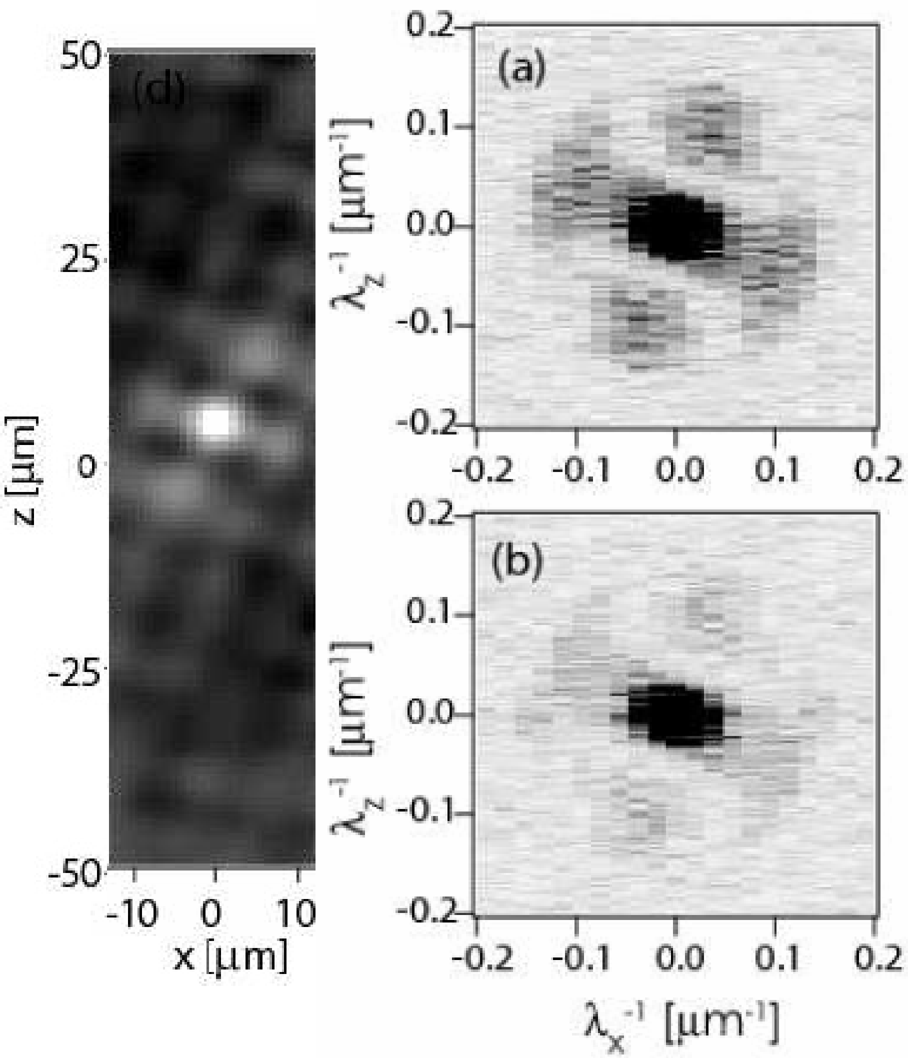

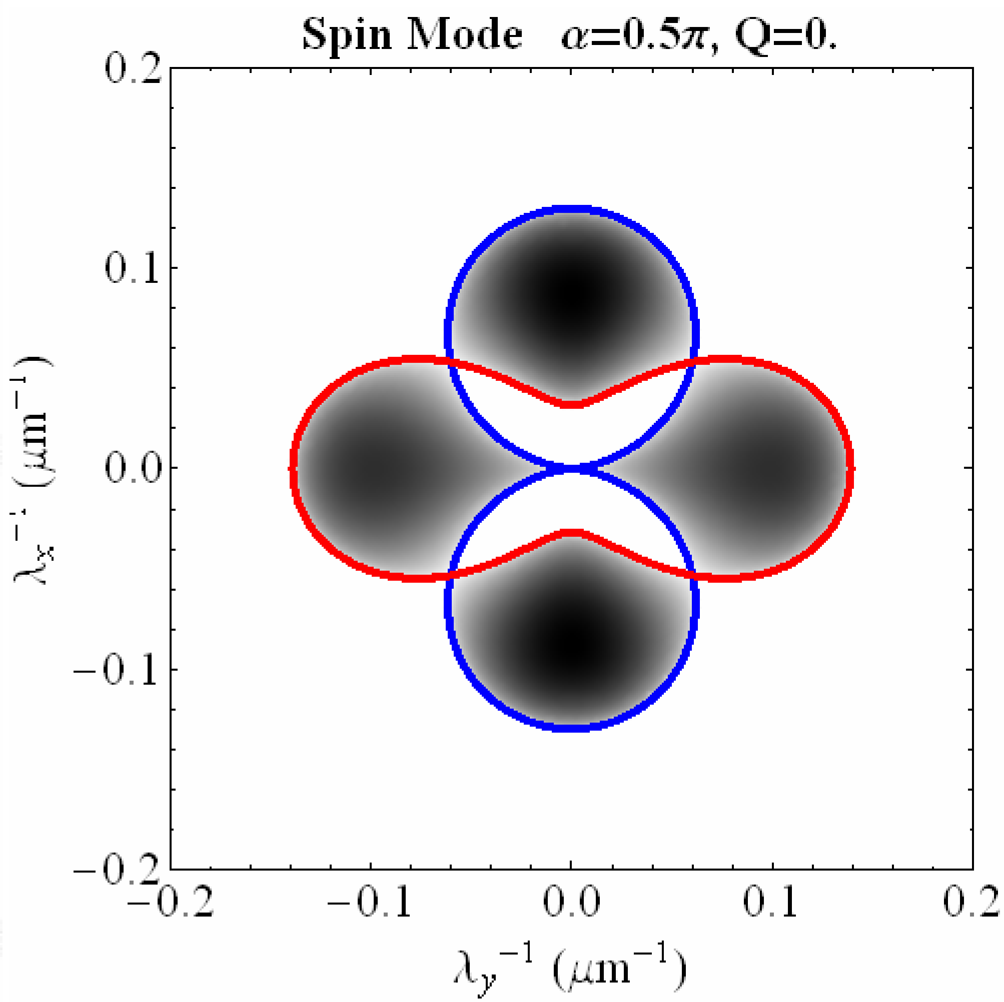

M. Vengalattore, et. al, arXiv:0712.4182

Dipolar interaction averaged after precession

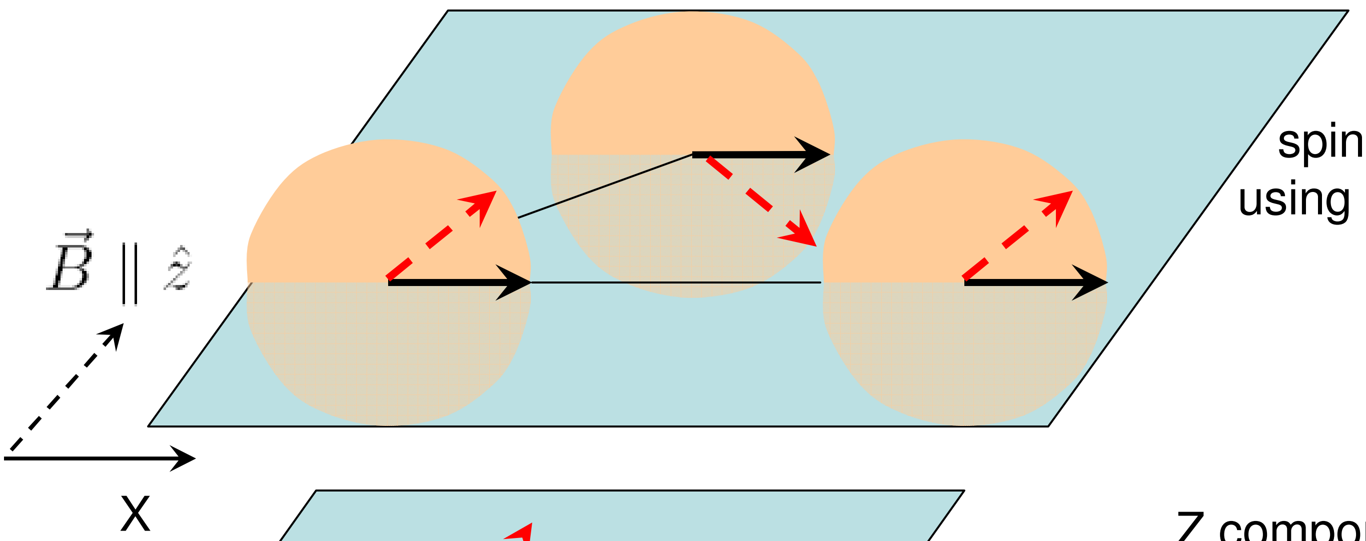

XY components of the spins can lower the energy using modulation along z.

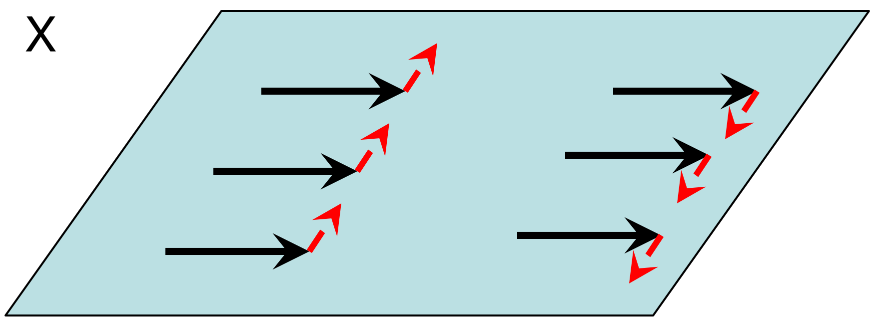

Z components of the spins can lower the energy using modulation along x

Instabilities of collective modes

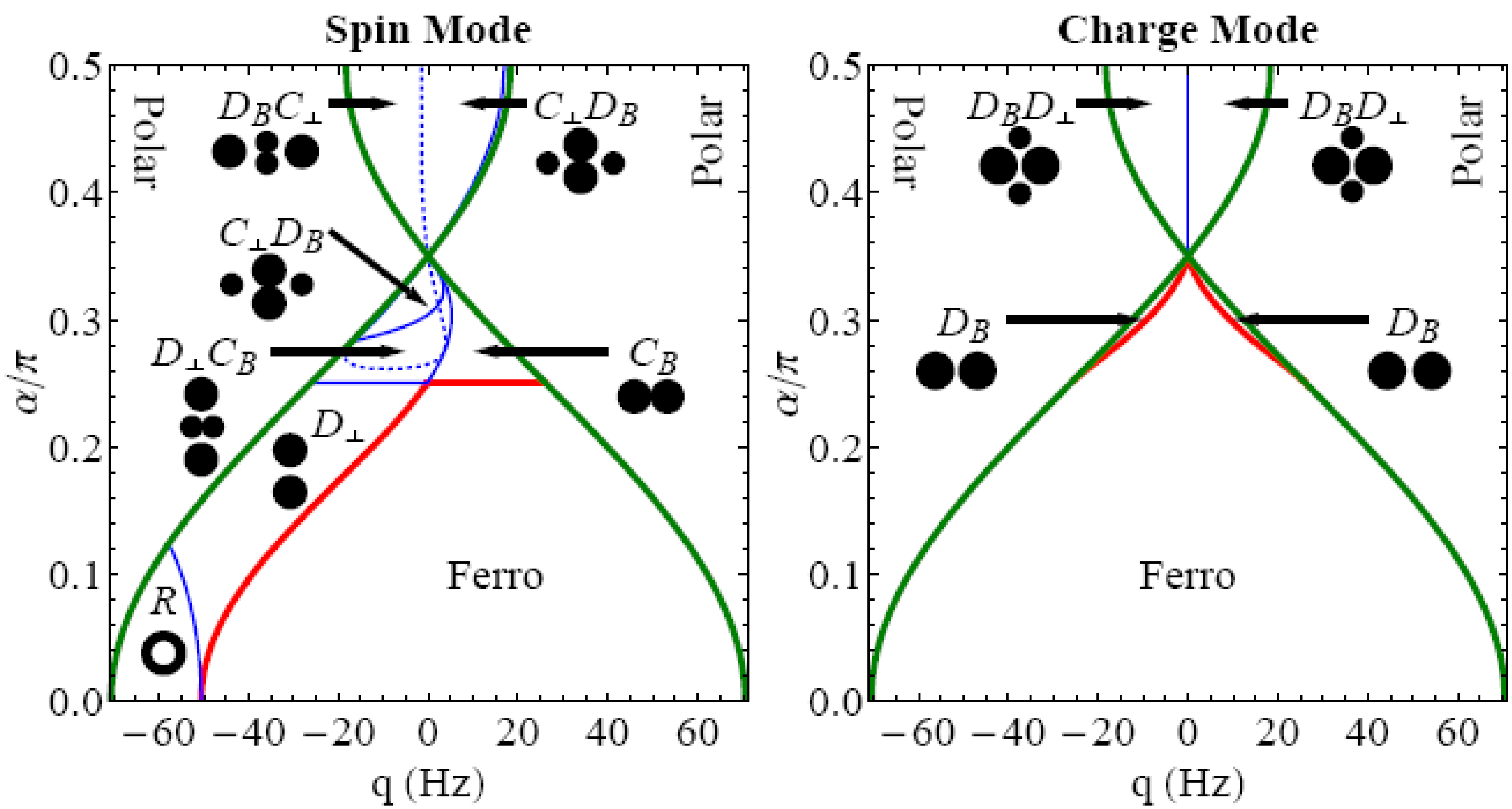

Instabilities of collective modes. Spiral configurations

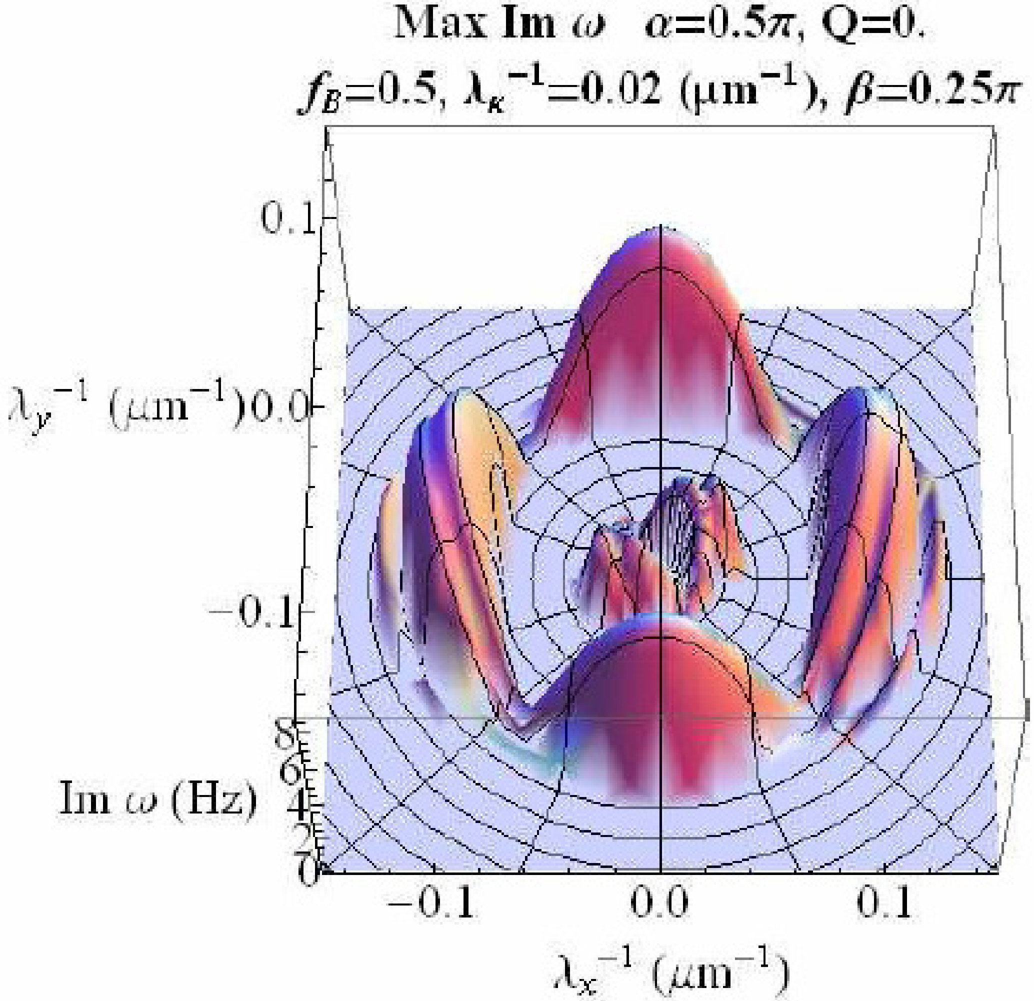

Spiral wavelength

$$\lambda_\kappa = 50\mu m$$

Spiral spin winding introduces a separate branch of unstable modes

Instabilities of the spiral state

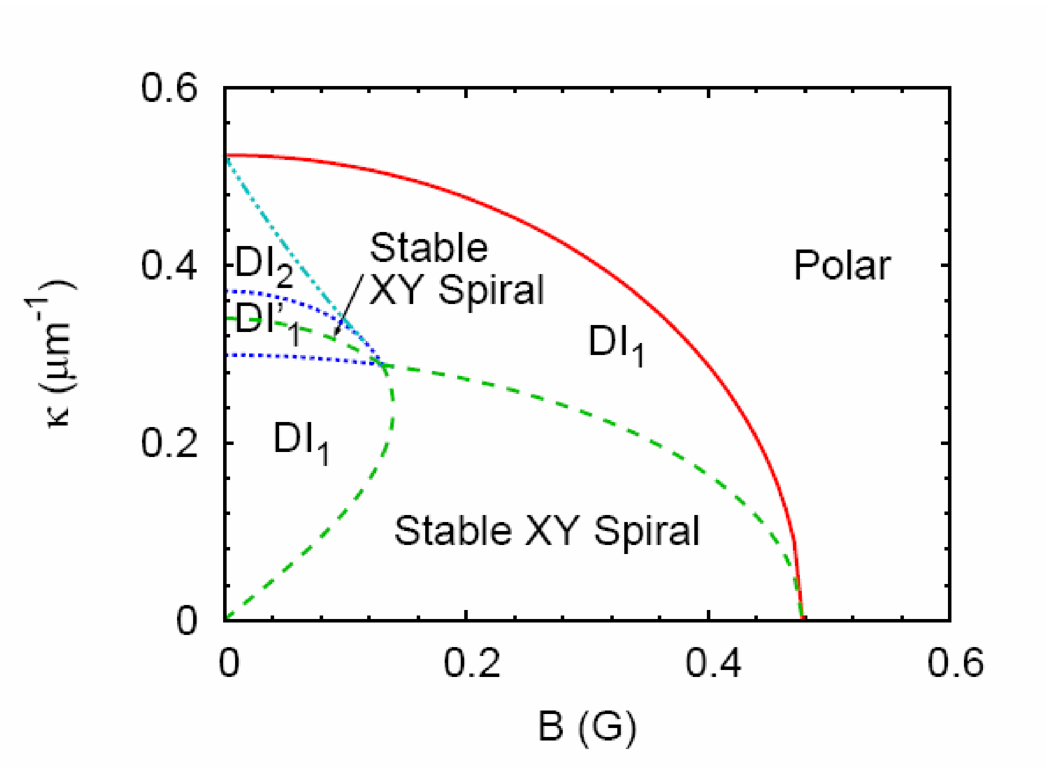

Adiabatic limit

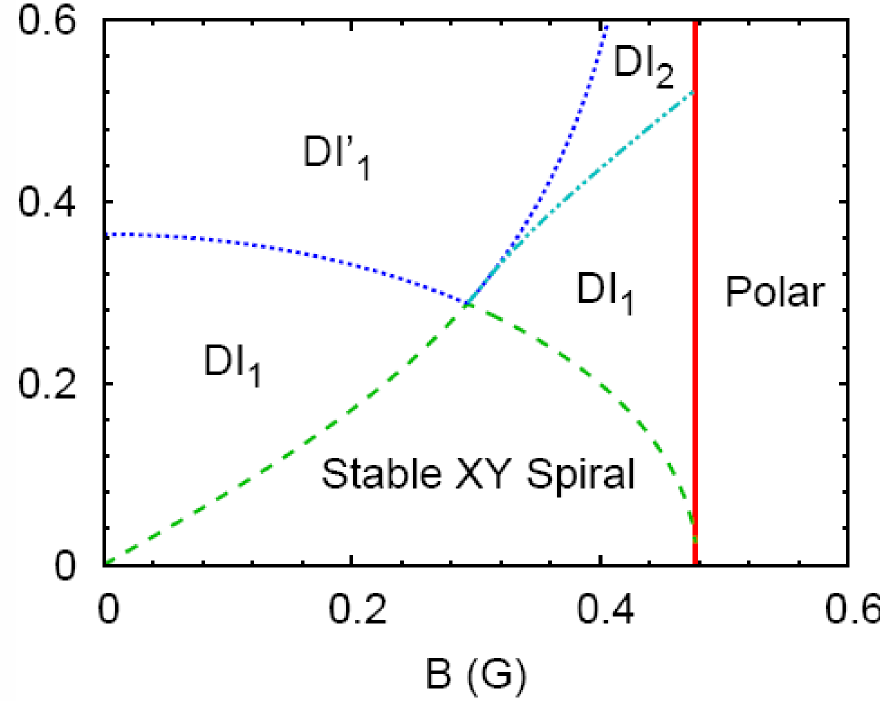

Sudden limit

Mean-field energy

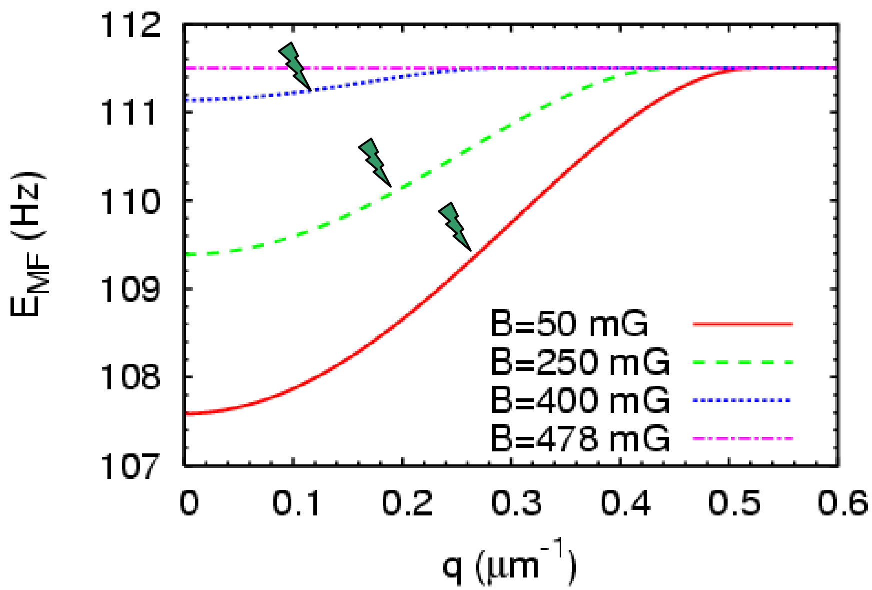

Inflection point suggests instability

Negative value of $\partial^2 E_{\mathrm{MF}}/\partial q^2$ shows that the system can lower its energy by making a non-uniform spiral winding

Uniform spiral

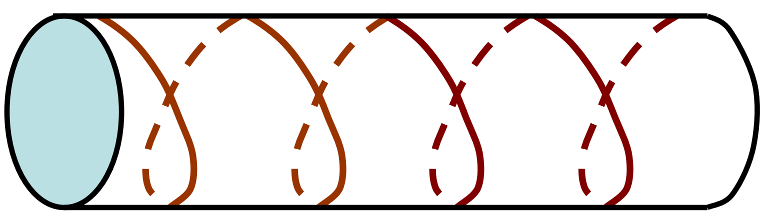

Non-uniform spiral

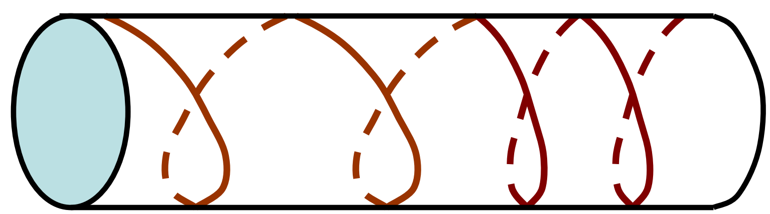

Conclusions

•Dipolar interactions crucial for spinor condensates…
•But effectively modified by quasi-2D and precession

•Variety of instabilities (ring, stripe, checkerboard)
•But what about the ground state?

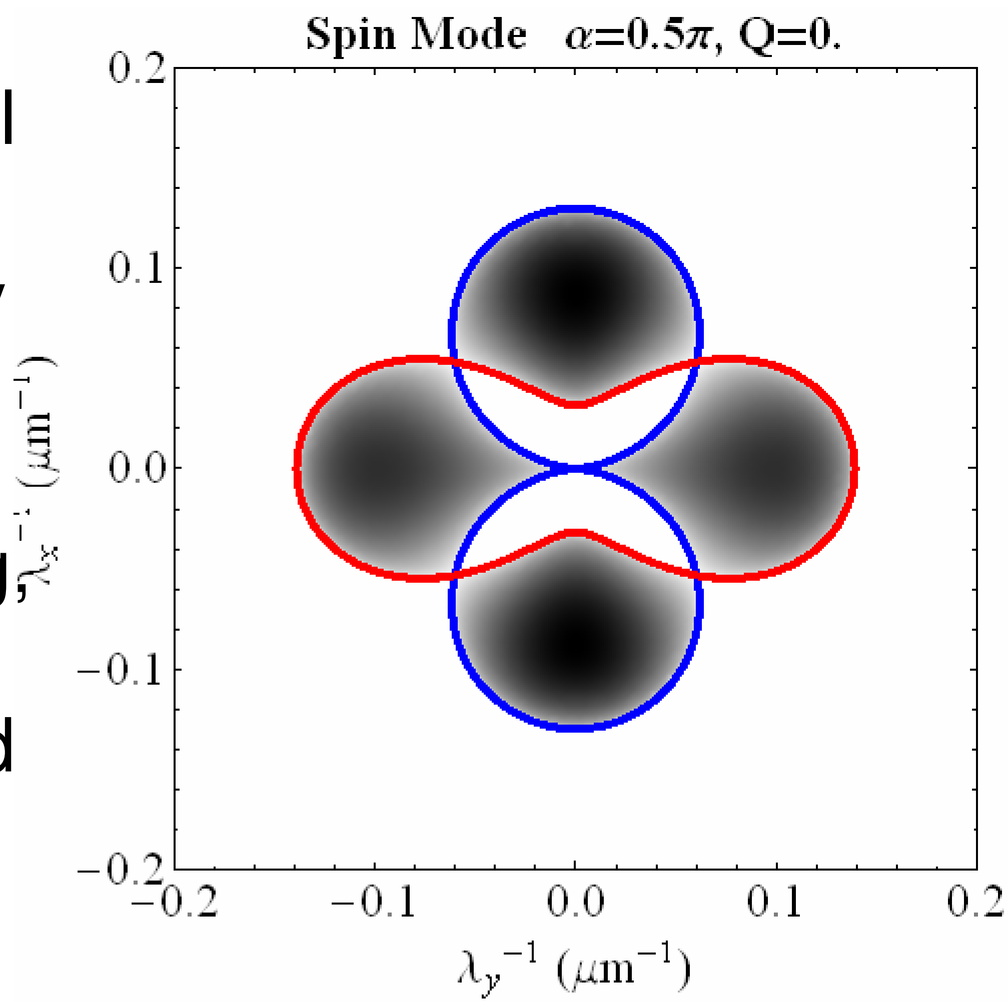

Nature of transiton and ordered phases